GLOBEX: WAVE DYNAMICS ON A GENTLY SLOPING LABORATORY BEACH

Gerben Ruessink[1], Hervé Michallet[2], Philippe Bonneton[3], Dominique Mouazé[4], Javier L. Lara[5], Paulo A. Silva[6], and Peter Wellens[7]

Abstract

As waves approach the shore, non-linearity in their dynamics becomes increasingly important. Most of our understanding of wave non-linearity has resulted from theoretical work, laboratory experiments and field studies on beaches slopes steeper than about 1:40. Here, very strong non-linear processes happen locally and on a short time scale, as demonstrated by narrow surf zones with plunging or collapsing breakers. The non-linearity on lower sloping beaches, typical of high-energy dissipative environments, has a different character, as it can now build up over a long period of time in a cross-shore extensive area. This second case of strong non-linearity is not well understood. This contribution serves to introduce the GLOBEX project, during which a high-resolution (in space and time) data set of the cross-shore evolution of short and infragravity waves was collected on a low-sloping (1:80) non-mobile laboratory beach for a range of wave conditions. Various other presentations at the conference will build on this introductory contribution.

Key words: wave transformation, laboratory experiments, swash, boundary-layer dynamics, numerical modelling

1. Introduction

Morphological change in the nearshore zone arises from the complicated interplay of water motion, sediment (sand) transport, and the morphology itself. The governing water motion, predominantly short (2 – 15 s) waves and wave-induced processes, contains strongly non-linear aspects. This non-linearity is obvious from, for example, the increasingly non-sinusoidal shape of short waves as they approach the shore through the shoaling and breaking zone (e.g., Elgar and Guza, 1985), and the generation of infragravity waves (e.g., Herbers et al., 1994, 1995), oscillatory motions in the sea surface with periods of 20 to 200 s. The non-linearity in the water motion is crucial to sediment transport. Non-sinusoidal short waves are the dominant mechanism responsible for onshore sediment transport under mild weather conditions (e.g., O'Donoghue and Wright, 2004; Ribberink and Al-Salem, 1994; Ruessink et al., 2011; Van der A et al., 2010). Infragravity waves can dominate the water motion close to the shore during more adverse weather (e.g., Guza and Thornton, 1982; Ruessink et al., 1998; Ruggiero et al., 2004; Sénéchal et al., 2011), and are important to beach and dune erosion (e.g., Russell, 1993; Van Thiel de Vries et al., 2008).

Wave non-linearity is paramount on both steep and low-sloping beaches, but is of different character. While on steep beaches very strong non-linear processes happen locally and on a short time scale (as demonstrated by narrow surf zones with plunging or collapsing breakers), the non-linearity on low-sloping beaches is significant because it builds up over a long period of time in a cross-shore extensive area. This second case of strong non-linearity is not well documented; most of our understanding and predictive ability of nearshore processes have resulted from theoretical work, laboratory experiments, and field

[1]Dept. Physical Geography, Faculty of Geosciences, Utrecht University, The Netherlands. b.g.ruessink@uu.nl
[2]LEGI, University of Grenoble, France. herve.michallet@legi.grenoble-inp.fr
[3]UMR EPOC, University of Bordeaux, Avenue des Facultés, Talence 33405, France. p.bonneton@epoc.u-bordeaux1.fr
[4]Laboratoire Morphodyn. Continentale et Côtière, Université de Caen, France. dominique.mouaze@unicaen.fr
[5]Environmental Hydraulics Institute "IH Cantabria", Universidad de Cantabria, Spain. jav.lopez@unican.es
[6]CESAM & Department of Physics, University of Aveiro, Portugal. psilva@ua.pt
[7]Deltares, The Netherlands. peter.wellens@deltares.nl

studies on beaches with slopes steeper than about 1:40. Within this context, a team including researchers from 9 European institutes in France, Spain, Portugal, United Kingdom and the Netherlands, as well as an institute from Chile, obtained funding under the Hydralab IV programme to perform the GLOBEX project – Gently sLOping Beach Experiment – in the 110-m long, small-scale Scheldegoot (Scheldt Wave Flume) of Deltares, Delft, The Netherlands.

The overarching aim of the project was to collect a high-resolution (in space and time) data set of the cross-shore evolution of short and infragravity waves on a 1:80 concrete beach for a range of wave conditions. In more detail, we focused on infragravity-wave dynamics, wave propagation, and boundary-layer dynamics:

- Infragravity waves arise by the transfer of energy from the short waves, leading to a low-frequency motion that is 'bound' to the short-wave groups. Within the surf zone the bound wave is released, propagates onshore without dissipating its energy, and reflects seaward to form a cross-shore standing wave pattern. Recent field studies have demonstrated that, in contrast to steeper beaches, infragravity-wave dissipation cannot be ignored (De Bakker et al., sub judice). Reflection coefficients were observed to be less than 10 – 30% and, accordingly, a cross-shore standing pattern did not develop, except for the lowest infragravity frequencies (< 0.017 Hz). This potentially has large effects on the magnitude and rate of beach and dune erosion during a storm (Ruessink et al., 2012). The mechanism(s) underlying infragravity-wave dissipation (e.g., Henderson et al., 2006; Thomson et al., 2006; Van Dongeren et al., 2007) are not well understood.
- Wave celerity is a key parameter in the hydrodynamics-module of our models. For example, the equations of mass flux, energy flux, and wave dissipation include wave celerity. It is thus also a parameter in models aiming to predict the cross-shore evolution (including dissipation) of infragravity waves. Recently, Tissier et al. (2011) compared wave-celerity observations to predictions based on linear wave theory and on a number of non-linear predictors. The comparison was hampered by insufficient data, in particular wave heights, to drive the non-linear predictors; on the whole, the agreement between observed and measured celerity was rather poor, especially in the inner surf zone (i.e. where non-linearity is strongest). A major spin-off of an improved predictor would be to use it inversely to estimate depth. Wave celerity is relatively easy to obtain from various remote sensing techniques, such as optical video or radar imaging (e.g., Bell, 1999; Stockdon and Holman, 2000). The ability to invert wave celerity to depth – for which we need to invert the hitherto uncertain non-linear celerity predictors – would enable us to obtain depth information during high-wave energy conditions when traditional survey methods fail.
- Field observations are necessarily limited to velocities above the wave bottom boundary layer and cannot provide information on the velocities within the boundary layer that are so relevant to the bed shear stress, steady streaming and net sediment transport. As waves propagate to shallow water, the wave shape and the near-bed wave velocity time series become non-linear (i.e., skewed and/or asymmetric), causing onshore sediment transport. Another mechanism that can cause onshore transport is non-linear boundary layer streaming, which is amplified by wave groupiness (Yu et al., 2010). In many models aiming to predict coastal evolution, the hydrodynamics in the wave boundary layer are parameterized by relating water-surface elevation to a 'representative' near-bed oscillatory motion. It is far from trivial how this should be done under strongly non-linear breaking waves (e.g., Abreu et al., 2013), as the skewness and the asymmetry of the orbital motion change in the vertical, especially in the wave bottom boundary layer (e.g., Berni et al., in press).

We believe that our new laboratory data set is crucial to not only improve our understanding of wave transformation, but will also enable rigorous testing of existing hydrodynamic models, and will eventually assist in the further development of models aiming to predict sediment transport and coastal evolution under high-energy wave conditions. As such, the GLOBEX project has the following 4 key objectives:

1. Identify the physical mechanism(s) leading to infragravity-wave dissipation;
2. Test and improve non-linear predictors for wave celerity;
3. Extend our knowledge of wave boundary layer dynamics, with a focus on non-linear boundary layer streaming and the vertical structure of velocity skewness and asymmetry; and,
4. Test and improve the capabilities of advanced hydrodynamic models in predicting cross-shore wave transformation.

Each objective is linked to a Work Package (WP), which, following WP1 – Coordination (led by University of Grenoble and Utrecht University), are WP2 – Infragravity-wave dissipation (led by Utrecht University), WP3 – Wave celerity (led by University of Bordeaux I), WP4 – Boundary layer dynamics (led

by University of Grenoble, in close cooperation with University of Aberdeen and University of Caen) and WP5 – Numerical modelling (led by Universidad de Cantabria). WP5 contains five models with different complexity. The inter-comparison of the models is of considerable interest to see how the assumptions in the governing equations affect model skill. Although we may expect the most advanced model, in our case based on the Reynolds-Averaged Navier-Stokes (RANS) equations (IH-2VOF; Lara et al., 2011), to perform best, this might not be the model to perform future sediment transport and bed-update computations, because of unrealistic computational demands. The obtained data and the advanced model(s) will aid in deriving parameterizations to overcome the limitations of the less advanced model(s).

In this paper we describe the GLOBEX project, including the experimental set-up, the experimental programme, and the instrumentation used. Also, we provide a general overview of the cross-shore transformation of various wave properties. An additional 6 papers will be presented at Coastal Dynamics 2013 that will cover results from the various WPs in GLOBEX (Almar et al., 2013; De Bakker et al., 2013; Rocha et al., 2013; Ruju et al., 2013; Tissier et al., 2013; Van der A et al., 2013).

2. Methods

2.1. *Experimental set-up*

The laboratory experiments were performed in the Scheldegoot (Scheldt Wave Flume) of Deltares, Delft, The Netherlands in April 2012. The flume is 110 m long, 1 m wide and 1.2 m high; it has glass windows along most of its length. The piston-type wave maker, equipped with Active Reflection Compensation (ARC), can generate regular waves with a maximum height H of 0.4 m and irregular waves with a maximum significant height H_s of 0.25 m. An impermeable concrete beach with a 1:80 slope was constructed, with its toe at 16.57 m from the wave maker (in rest position, x = 0 m), see Figure 1. All experiments were run with a still water depth of 0.85 m over the horizontal approach; this implies that the still-water shoreline was at x = 84.57 m. The median grain size D50 of material that was laying loose on the concrete bed before the flume was filled with water was 0.75 mm; D10 and D90 amounted to 0.49 and 1.15 mm, respectively.

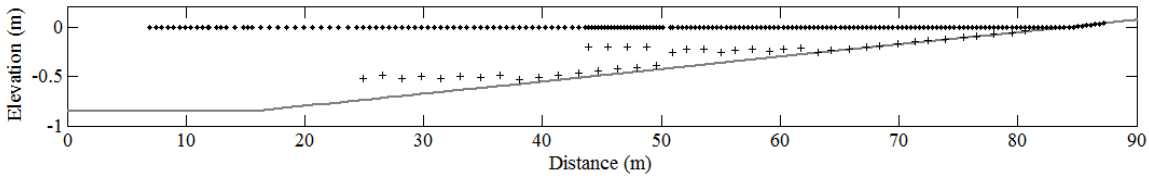

Figure 1. Bed elevation z versus cross-shore distance x in the Scheldegoot during the GLOBEX project. Here, x = 0 is the wave-maker location, while z = 0 corresponds to the still water level. The 190 dots are the positions of the wave gauges; the 43 pluses are the positions and heights above the bed of the electromagnetic current meters. The bed level was determined with a terrestrial laser scanner before the flume was filled with water.

2.2. *Experimental programme*

The programme comprised 8 wave conditions grouped in 3 test series with varying complexity to reach our objectives (Table 1).

- Series A involves random short waves in which the offshore H_s and peak period T_p were varied. A1 and A2 correspond to intermediate-energy and high-energy sea conditions, respectively, while A3 represents an energetic swell.
- Series B comprised 3 bichromatic wave cases. In B1 and B2, the frequencies of the primary components f_1 and f_2 were varied such that the difference frequency f_3 (= $f_2 - f_1$) decreased from 0.067 to 0.042 Hz but the amplitudes a_1 and a_2 were identical. Series B3 had the same f_1 and f_2 as B2, but the group modulation was enhanced by decreasing a_1 and increasing a_2. In all 3 cases the sum of a_1 and a_2 equaled 0.1 m, chosen because of H_s = 0.2 m in A2, and the mean frequency f_m equaled ≈0.44 Hz, the peak frequency (=1/T_p) of A2 and A3.
- Series C contained two single monochromatic wave cases. C1 was an infragravity-wave condition, with H = 0.02 m and period T = 23.8 s, identical to the group period (= 1/f_3) in B2 and B3. The

amplitude was determined during the test week prior to the actual experiments, as it provided approximately the same swash zone width (i.e., the distance between maximum wave run-up and run-down) as observed for series B3. C2 involved a monochromatic short-wave condition, with H = 0.2 m and T = 2.25 s.

The characteristics of Series A, B and C1 were designed specifically to unravel the mechanisms underlying infragravity-wave dissipation. In Series A, the infragravity-wave field is random (as is the case in the field), while in Series B a single infragravity-wave frequency (= f_3) is present only. The difference between B1 and B2 lies in the difference frequency, and that between B2 and B3 in the group modulation and hence the height of the incoming bound infragravity wave. C1 has the same infragravity-wave frequency as B2 and B3, but no short-infragravity-wave interaction. C2 was run to collect a high resolution velocity profile in the wave bottom boundary layer to estimate the bed roughness, see Van der A et al. (2013). Series B is also particularly suited for the study of wave celerity and of the velocities in the bottom boundary layer because the regular groups allow for ensemble averaging and, hence, more robust statistics compared to the random-wave cases of series A; see, for example, Tissier et al. (2013) and Van der A et al. (2013).

All wave-paddle steering signals in Series A and B were made with second-order wave generation. In Series A, the signals were based on a JONSWAP spectrum with a peak enhancement factor γ of 3.3 for A1 and A2, and of 20 for A3 to provide a narrow-banded (in frequency) spectrum for the swell waves. For C1, second-order wave generation was not possible because the chosen period fell outside the range of validity of the second-order wave generation theory. Because the wave height and steepness were so small, the use of first-order wave generation was considered adequate for C1. The Automated Reflection Compensator (ARC) was turned on to minimize reflections from the wave paddle. The signals of A and B had a total duration of 75 minutes; the signal of C1 was 30 minutes long.

Table 1 Overview of wave conditions

Test series A					
	H_s (m)	T_p (s)			Remark
A1	0.10	1.58			JONSWAP, γ=3.3; prototype: H_s = 2 m; T_p = 7 s
A2	0.20	2.25			JONSWAP, γ=3.3; prototype: H_s = 4 m; T_p = 10 s
A3	0.10	2.25			JONSWAP, γ=20; prototype: H_s = 2 m; T_p = 10 s
Test Series B					
	a_1 (m)	a_2 (m)	f_1 (Hz)	f_2 (Hz)	Remark
B1	0.09	0.01	6/15	7/15	$1/f_3$ = 15 s; f_m = 0.433 Hz
B2	0.09	0.01	0.42	0.462	$1/f_3$ = 23.8 s; f_m = 0.441 Hz
B3	0.07	0.03	0.42	0.462	$1/f_3$ = 23.8 s; f_m = 0.441 Hz
Test Series C					
	H (m)	T (s)			Remark
C1	0.02	23.8			
C2	0.20	2.25			Ran for the study of the wave bottom boundary layer only

2.3. *Instruments and measurements*

A wide suite of instruments was deployed during the experiments (Figure 2).

- **Waves** – Sea-surface elevation was measured using 21 wave gauges (WGs), 18 of which were mounted on 3 movable trolleys. The inshore trolley contained 11 capacitance WGs separated by 0.37 m, 3 of which were co-located with an electromagnetic current meter (EMCM) to measure horizontal and vertical free-stream flow velocities. The middle trolley had 5 resistance-type WGs, spaced 0.55 m, and 2 EMCMs, while the offshore trolley had 2 resistance-type WGs, spaced 2.2 m, and no EMCMs. The remaining 3 resistance-type WGs were mounted individually near the wave maker. All data from the WGs and EMCMs were collected at 128 Hz by the central Scheldegoot data acquisition system. The height of the EMCMs above the bed varied between 0.01 m and 0.3

m, depending on location within the flume (see Figure 1). In addition, the sea-surface elevation was also imaged at 20 Hz using 2 video cameras looking sideways through the glass windows and by a single video camera looking obliquely from above. The wave-paddle motion was stored too to be used as input in numerical models with an internal wave maker.

- **Swash** – Instruments focusing specifically on swash motions comprised a single downward looking video camera (sampling at 20 Hz), a swash-wire mounted ≈1cm above the bed (sampling at 128 Hz), a RIEGL VZ-400 terrestrial laser scanner, and an acoustic Doppler velocimeter (ADV).
- **Boundary-layer dynamics** – Equipment to measure horizontal and vertical velocities inside the wave bottom boundary layer comprised a Deltares Laser Doppler Velocimeter (LDV) and a Dantec Laser Dopper Anemometry (LDA) system at x = 60.6 m and x = 69.3 m, respectively. The LDV is a forward-scatter system; its measurement volume can be translated along the vertical z-axis with a precision of 0.1 mm. The vertical translation precision of the LDA was 0.05 mm. At the LDV, an ADV was operated to obtain velocity data above the wave bottom boundary layer. The output of a WG not included in the aforementioned 21 WGs was used to measure sea-surface elevation at the location of the LDA. Silver-coated hollow glass spheres with a diameter of 10 μm were used to seed the flow, except during the first few days of the experiment when seeding material was unavailable. For additional details on the LDV and LDA, see Van der A et al. (2013).

Figure 2. Photos showing the flume and various instruments deployed during GLOBEX. (a) Overview of the 110-m long flume in down-wave direction. (b) Trolley, instrumented with 11 wave gauges and 3 electromagnetic current meters; (c) Side-looking camera. (d) Acoustic Doppler velocimeter deployed in the swash zone; (e) Part of the Dantec LDA optics and traverse system; (f) Deltares LDV system; (g) Riegl VZ-400 Terrestrial Laser Scanner. All photos except (d) taken by B.G. Ruessink; photo (d) by Dominic van der A.

The first 7 wave conditions (A1-C1) were run consecutively as a single session. Data of the WGs and EMCMs were collected starting 1 minute prior to wave activity until 15 minutes after wave activity had ceased, resulting in 91-minute and 46-minute long data blocks for Series A/B and C1, respectively. During the final 15 minutes, the ARC remained turned on. As a consequence, any remaining motion disappeared within several minutes; thus, the 15-minute rest period was sufficient to guarantee that the next case was

started with perfectly still water. Every morning, before the start of the first case, the water level in the flume was restored to 0.85 m above the horizontal approach. Because of leakages, the water level could drop by a few mm overnight. Once a session was completed, most instruments were relocated either along the flume or, when fixed to a single horizontal position, adjusted vertically. Each session of 7 cases was repeated 10 times. In this way, data of sea-surface elevation were collected at 190 WG positions, from near the wave maker (x = 6.96 m) to the upper limit of the swash zone (x = 87.25 m), with a spacing ranging from 0.074 to 0.75 m (Figure 1). The WG at x = 6.96 m was not moved to confirm that the time series of sea-surface elevation for each condition was indeed identical in the 10 different sessions (Figure 3). Velocity data (EMCMs) were acquired at 43 positions (Figure 1). The 10 sessions were combined and synchronized into one data set for each wave condition. The EMCM and WG data collected seaward of the swash zone were zeroed by setting the mean of the first minute to 0. In general, the offset of the resistance type WGs was less than 0.002 m. The minimum value of the WG data collected within the swash zone was set to the bed level, assuming the bed to be dry in that instance; values estimated to be within 3 mm of the bed were flagged as "bad" and were not used in any subsequent computations. Finally, the effective WG and EMCM record length was set to 69 minutes for Series A and B, and 24 minutes for Series C1, by removing the first 6 and final 16 minutes of the original data blocks. Because of time constraints, the full 91 minutes were not available for series A and B in the tenth session. Therefore, the effective length of the WG and EMCM time series measured in this session was restricted to 39 minutes for Series A and to 24 minutes for Series B.

For Series A and B, LDA measurements were done at 18 elevations logarithmically spaced between z = 0.1 mm and 10 mm during the 10 sessions, while for series C the spacing reached up to 50 mm above the bed, consisting of 12 elevations. C2 was run for one full day, during which data were collected at 30 elevations between 0.1 and 50 mm above the bed. Preliminary analyses (Van der A et al., 2013) suggest that all LDA data (A1-C1) were collected in the transitional regime between laminar and turbulent flow.

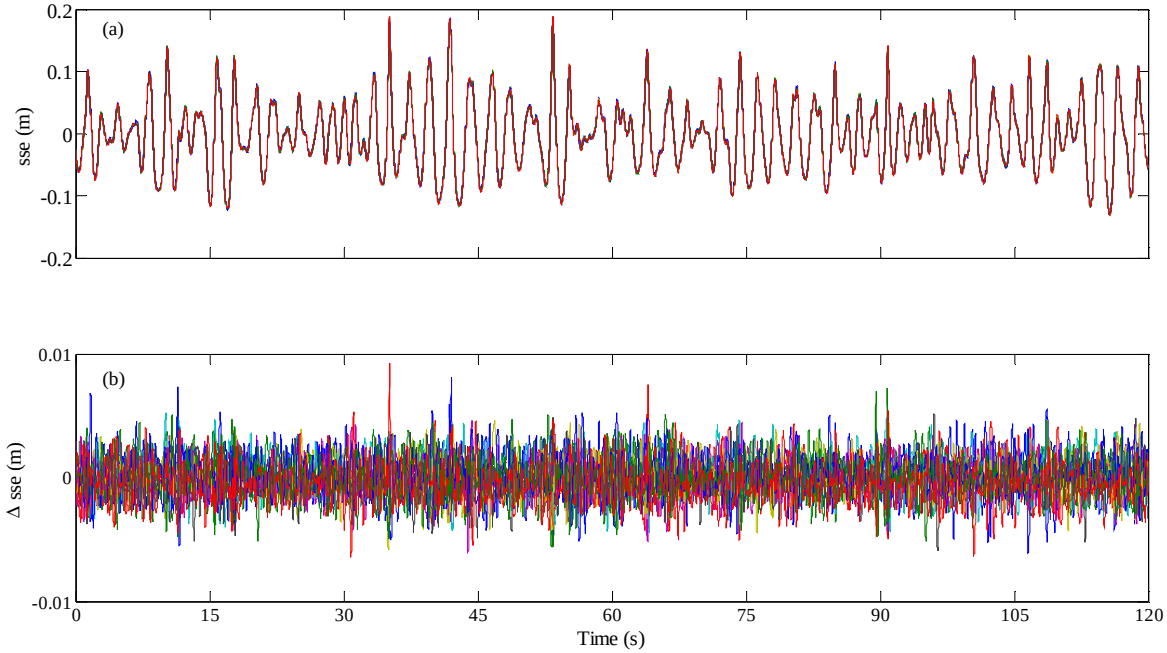

Figure 3. (a) Measured sea-surface elevation (sse) at x = 6.96 m versus time for all 10 sessions (condition A2). The 10 lines are virtually indistinguishable, indicating the near-perfect repetition of the wave-paddle motion in each session. (b) Difference in sea-surface elevation, Δsse, between the 10 individual runs and the mean of the 10 runs (condition A2) versus time. As can be seen, | Δsse| was typically less than 5 mm and did not systematically vary with time. As A2 was the most energetic wave condition, values of |Δsse| were generally less than 2-3 mm for all other conditions.

3. Preliminary results

Various results are discussed by other papers presented during the Coastal Dynamics 2013 conference:

- De Bakker et al. − infragravity-wave dissipation;
- Rocha et al. – non-linearity of short and long waves;
- Almar et al. and Tissier et al. – short-wave celerity;
- Van der A et al. – wave boundary layer dynamics; and,
- Ruju et al. – swash motions.

Here, some results obtained with the WGs and EMCMs are presented to provide an overview of the observed cross-shore evolution of the short and infragravity waves in series A.

Figure 4 shows a 2-minute long time-space diagram of the sea-surface elevation of condition A2, together with the approximate location of the swash and backwash motion as determined with the swash wire. The cross-shore evolution of the significant wave height in the short-wave and infragravity-band, together with the mean water level (set-down/up), of A1, A2 and A3 are given in Figure 5. Time series of sea-surface elevation at selected locations are provided in Figure 6 to further aid in the interpretation of Figure 4. The variance-density spectra, calculated using 3-minute long, 50% overlapping, Hamming-windowed blocks, of these 4 series are shown in Figure 7. Finally, the short-wave skewness and asymmetry of all three A conditions are shown in Figure 8. In the computations, the separation between the short-wave and infragravity-wave frequency band was set to 0.37 Hz for A1, and 0.26 Hz for A2 and A3, corresponding to a valley in variance density near the toe of the slope (for A2, see Figure 7, x = 16.2 m). The upper frequency limit of the short-wave band was taken as 15 Hz.

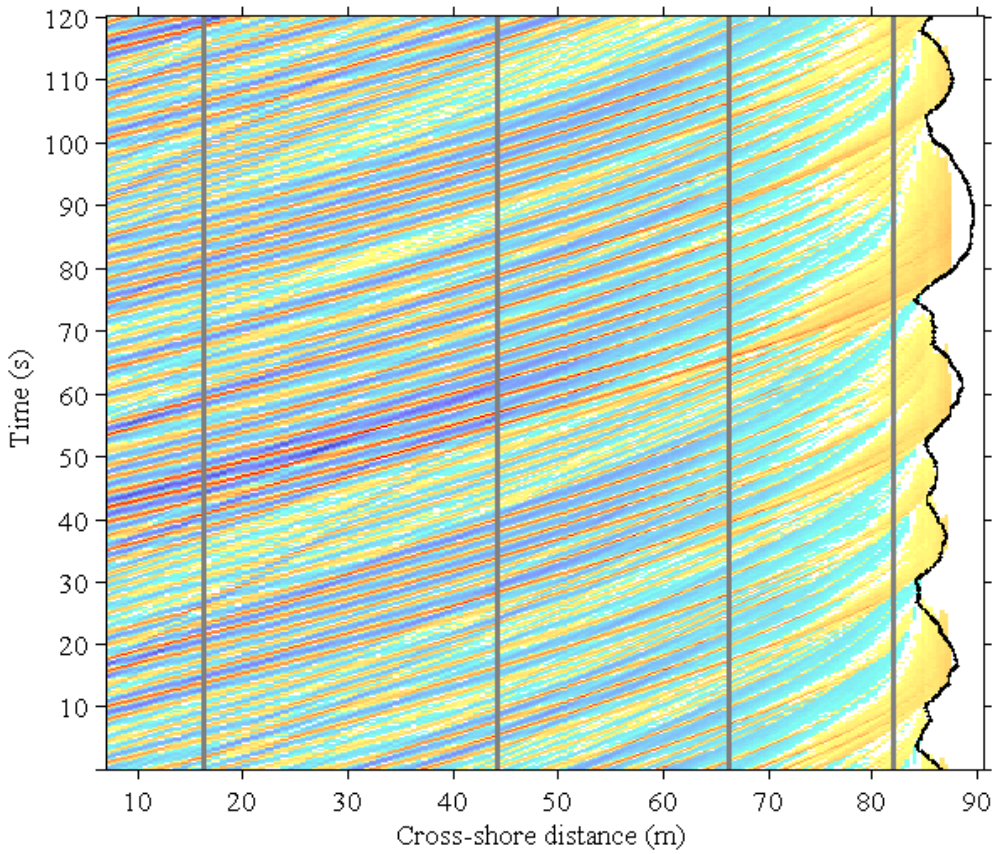

Figure 4. Two-minute time-space diagram of the sea-surface elevation measured during condition A2. Warm (red) colours correspond to values above 0 (the still water level), cold (blue) colours to values below 0.The black line fluctuating around x ~ 84 m is the run-up located determined with the swash wire. The four vertical gray lines represent the locations of the time series shown in Figure 6, and are (from left to right) near the toe of the slope (x = 16.2 m), the location where the largest waves started to break (x = 44.1 m), the location from which all short waves broke (x = 66.2 m), and a location just seaward of the swash zone (x = 81.7 m).

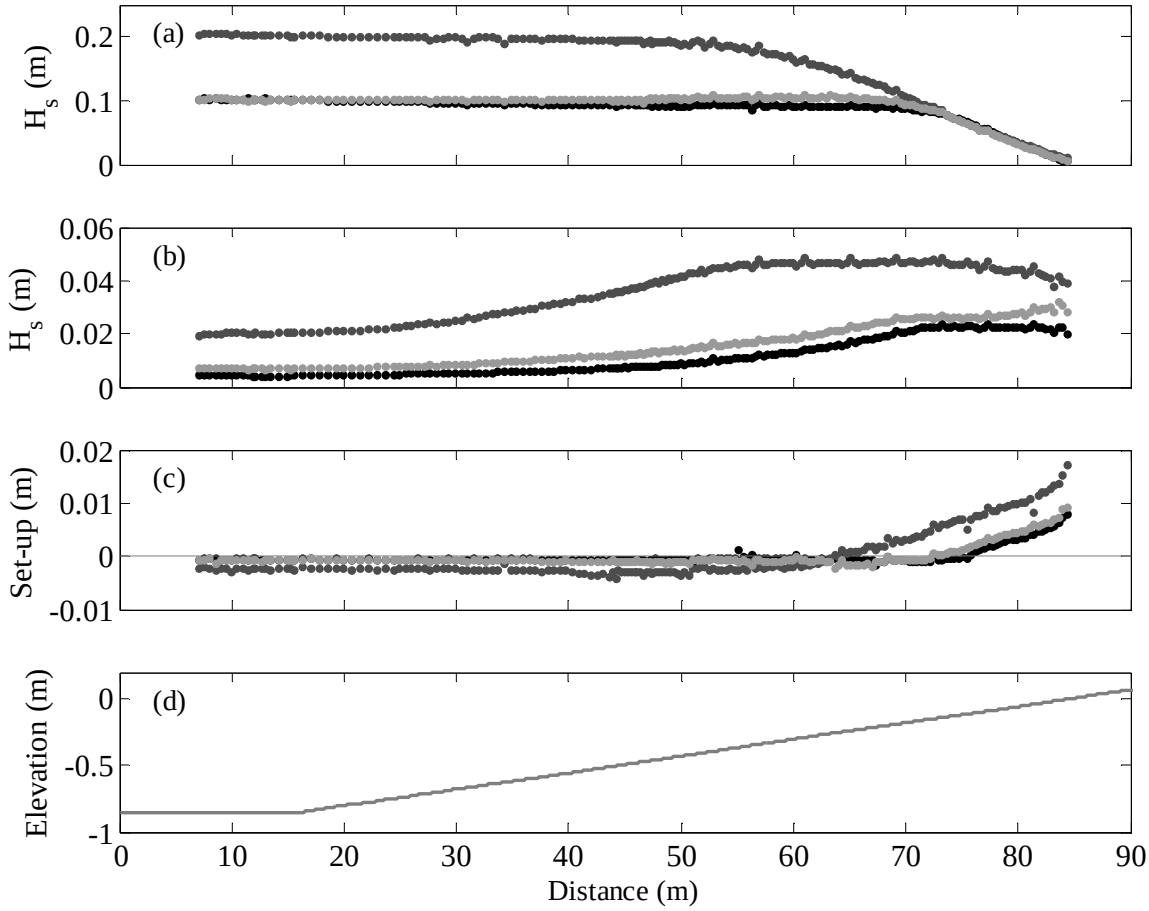

Figure 5. (a) Short-wave significant wave-height, (b) infragravity-wave significant wave height and (c) mean water level versus cross-shore distance *x*. Panel (d) shows the bed profile for reference. In (a)-(c), the black dots are A1, the dark-gray dots are A2 and the light-gray dots are A3. Values from time series collected within the swash zone are not shown.

The short waves dominated the wave field across the entire profile except for the innermost part of the surf zone (Figures 4-7). There, the surf zone was saturated: the significant short-wave height was no longer controlled by the offshore wave height but by the local water depth (Figure 5a, x > ~72 m), with the ratio of the significant short-wave height to the water depth amounting to approximately 0.5-0.6. Also, the infragravity motion started to affect the propagation of individual short waves in the saturated surf zone, as can be seen clearly for x ~ 70-80 m in Figure 4 for A2. Individual bores started to capture each other by infragravity-scale modulations of the water depth (see Tissier et al., 2013 for further details), resulting in a concentration of short waves on the infragravity-wave crests and the near-absence of short waves in the infragravity-wave troughs (see Figure 6d). In all conditions, the swash was completely dominated by infragravity motions.

The significant infragravity-wave height was constant over the horizontal approach for all conditions, to then increase over the sloping up to the outer edge of the surf zone (x ~ 52 m during A2, and x ~ 70 m during A1 and A3). Within the surf zone, the infragravity-wave height remained approximately constant, to finally decrease slightly toward the swash zone. Figure 5b challenges the common viewpoint that infragravity waves grow in height throughout the surf zone to reach their maximum height in the swash. Further analyses in De Bakker et al. (2013), in which the total infragravity signal was decomposed into incoming and outgoing signals, demonstrate that the rapid growth and its surf-zone arrest were primarily due to the incoming infragravity waves. The height of the outgoing infragravity waves decreased in the offshore direction as expected from the de-shoaling of free infragravity waves propagating at $\sqrt{(gh)}$,

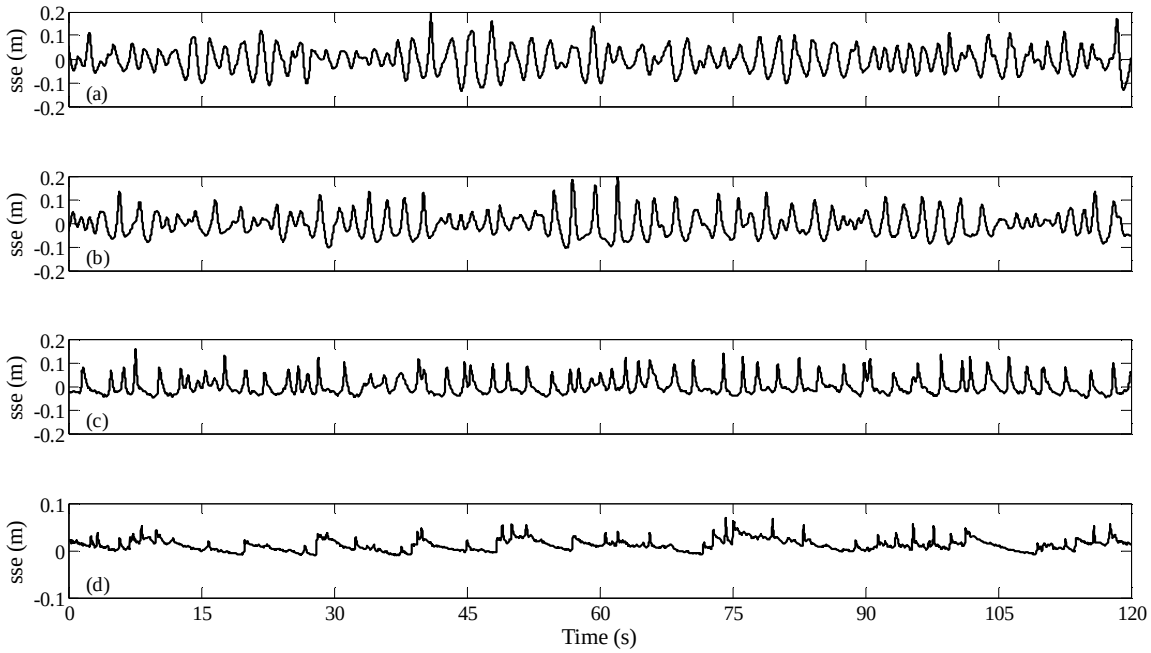

Figure 6. Sea-surface elevation sse (condition A2) versus time near (a) the toe of the slope (x = 16.2 m), (b) outer surf zone (x = 44.1 m), (c) inner surf zone (x = 66.2 m) and (d) just seaward of the swash zone (x = 81.7 m). Note the different vertical scale in (d). The four locations are indicated with the vertical gray lines in Figure 4.

where g is gravitational acceleration and h is the water depth.

The spectra in Figure 7 demonstrate that as the waves shoaled from the toe of the slope toward the outer surf zone (here, from x = 16.2 to 44.1 m) the variance density at the peak frequency reduced slightly, while the overall spectrum broadened with an increase in variance density particularly at the infragravity frequencies (here, f < 0,26 Hz) and at twice the peak frequency (f ~ 0.8-0.9 Hz). This evolution is indicative of non-linear energy transfer (triad interactions) to both higher and lower frequencies (e.g., Herbers et al., 2000). Further onshore, within the surf zone, the variance density at the primary frequencies reduced more rapidly, with a small reduction in the peak frequency, while elsewhere the variance density still increased. Just seaward of the swash zone, the spectrum increased monotonic with decreasing frequency well into the infragravity band (f ~ 0.05 Hz), indicating that also at these infragravity frequencies dissipation must have been considerable. Note that from x = 61.2 to 81.7 m the variance density at intermediate infragravity frequencies (0.03-0.05 Hz) remained approximately constant, while only that at lower frequencies increased. Interestingly, the infragravity part of all 4 spectra shown did not contain spectral peaks and valleys indicative of cross-shore standing pattern. De Bakker et al. (2013) use a

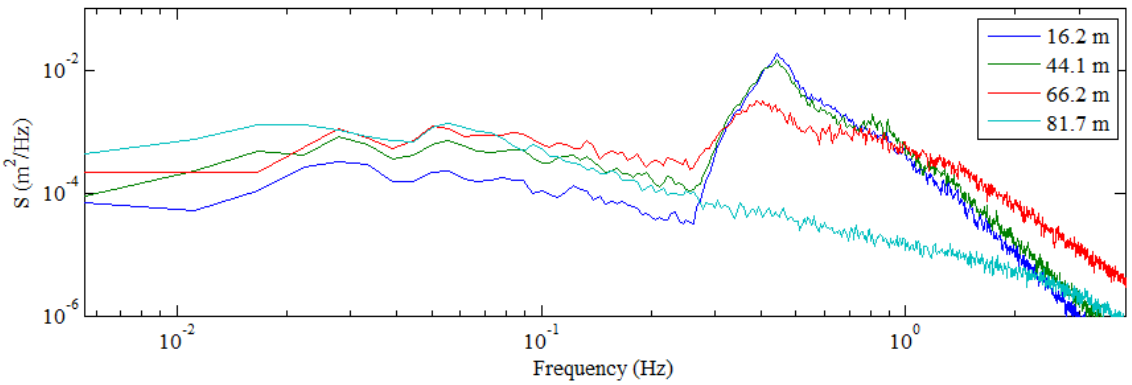

Figure 7. Spectral variance density S versus frequency f at the four locations shown in Figure 5 (condition A2)

frequency-domain complex eigenfucntion analysis of the data to demonstrate that such a standing pattern is indeed restricted to the lowest infragravity frequencies; the higher infragravity frequencies were onshore propagating, indicating that their energy was indeed dissipated in the surf zone. Interestingly, the infragravity waves developed a distinct sawtooth shape in the innermost part of the surf zone (e.g., Figure 6d), similar to the sawtooth pattern of breaking short waves (bores). Similar infragravity-wave shapes were observed in the laboratory by Van Dongeren et al. (2007), who interpreted this as infragravity-wave breaking.

Figure 8 illustrates that, during shoaling, the short waves became increasingly skewed. The skewness reached maximum values of 1.5 to 2 in the outer to mid shoaling zone, and then decreased rapidly to 0 as the waves became asymmetric (saw-tooth, $x > 80$ m). For the most energetic condition (A2) the skewness started to increase at more seaward locations than for A1 and A3; the largest skewness, however, was observed for the high-period, narrow-banded swell (A3). When we compare Figure 7b to Figure 5a, we see that the waves already started to become asymmetric prior to the onset of wave breaking (e.g., x = 50-70 m for A1 and A3). Rocha et al. (2013) show that the skewness and asymmetry of the short-wave orbital motion followed the same cross-shore trends as observed in Figure 8 for the sea-surface elevation.

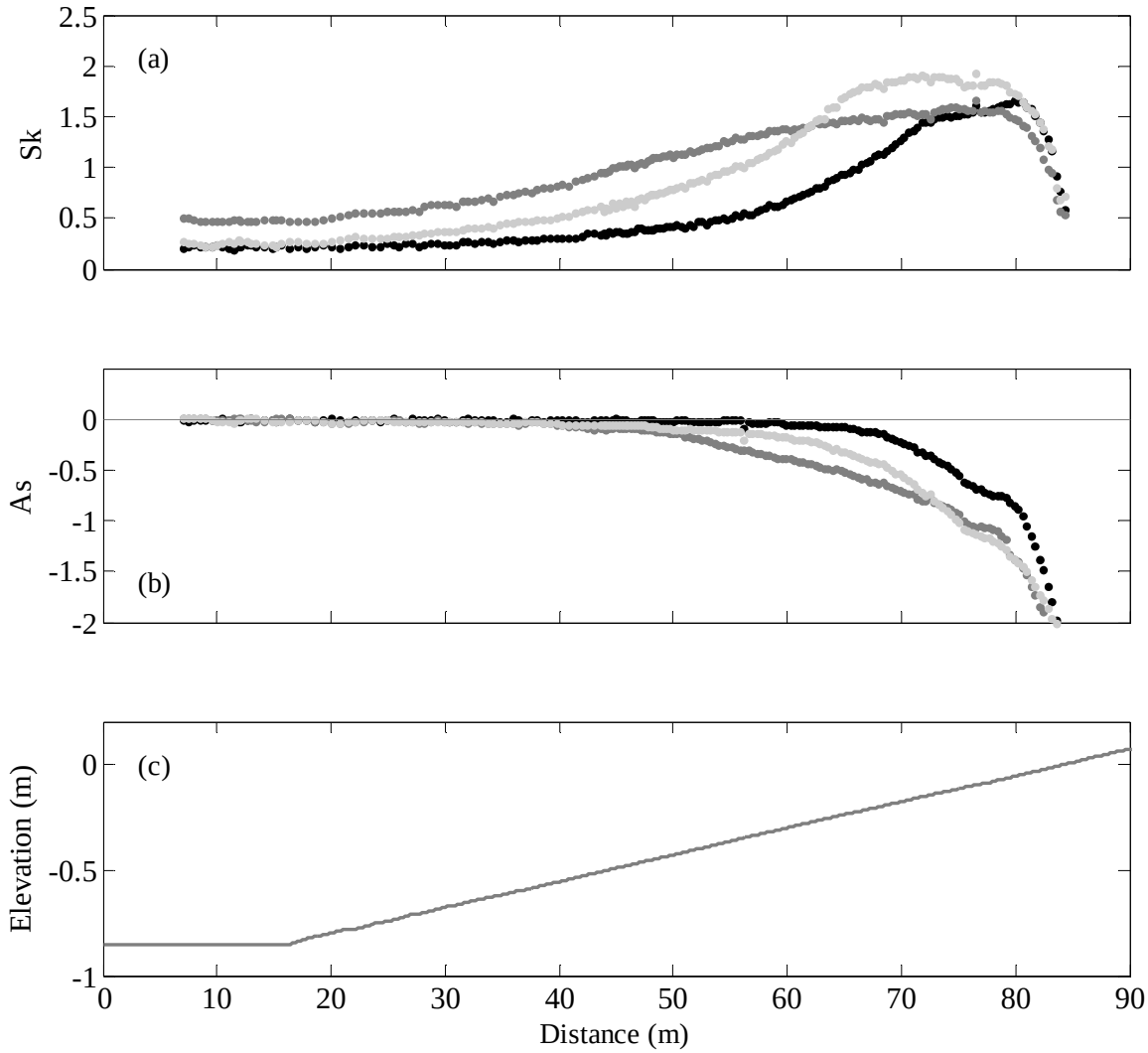

Figure 8. Short-wave (a) skewness and (b) asymmetry versus cross-shore distance. Panel (c) shows the bed profile for reference. In (a)-(b), the black dots are A1, the dark-gray dots are A2 and the light-gray dots are A3. Values from time series collected within the swash zone are not shown.

4. Concluding remarks

The GLOBEX experiment took place over an approximately 1 month period in April 2012. Almost 25 scientists from 10 institutes were involved, and c. 13 staff from Deltares performed technical support. The experiments resulted in a highly detailed data set of the cross-shore evolution of short and infragravity waves from well seaward of the surf zone up to and including the leading edge of the swash motion on a fixed 1:80 sloping beach. In addition, high-resolution observations of the horizontal and vertical flow in the wave bottom boundary layer were collected at two locations. The majority of the measurements were performed with traditional equipment including wave gauges and electromagnetic flow meters; however, additional measurements were performed with various instruments that have been introduced to the laboratory environment only recently. An example is the terrestrial laser scanner, which was set-up at the top of the beach (Figure 2a) to sample the swash/backwash motion and whose output will be compared with the results obtained from the more traditional approaches including the swash wire and the run-up detected from the video images.

Acknowledgements
We are greatly indebted to the Deltares technicians and staff members (Frank van Eeden, John Coolegem, Pieter Pasterkamp, Frans de Vreede, Richard Boele, Rob Hoffman, Jaap de Schipper, Paul Meys, Job Waaijerink, Hans Deutekom, Jelle Molenaar, Ivo Wenneker and Irv Elshoff) for their excellent support during the experiments. It was a pleasure to work with you! We also wish to thank all other GLOBEX team members (Eric Barthélemy, Laure Vignal, Céline Berni, Marcel van Maarseveen, Anouk de Bakker, Marion Tissier, Mariana Rocha, Tiago Abreu, Florent Birrien, Nadia Sénéchal, Vincent Marieu, Dominic van der A, Rafael Almar, Rodrigo Cienfuegos, Andrea Ruju, Giovanni Coco, and Iñigo Losada Rodriguez) for their help in preparing the original proposal, their excellent work to collect the GLOBEX data set, and for making the stay in Delft such a pleasant and memorable occasion. The GLOBEX project was supported by the European Community's Seventh Framework Programme through the grant to the budget of the Integrated Infrastructure Initiative Hydralab IV, EC contract no. 261520.

References

Abreu, T., Michallet, H., Silva, P.A., Sancho, F., Van der A, D. and Ruessink, B.G., 2013. Bed shear stress under skewed and asymmetric oscillatory flows. *Coastal Engineering*, 73: 1-10.

Almar, R., Bonneton, P., Michallet, H., Cienfuegos, R., Ruessink, G. and Tissier, M., 2013. On the use of the Radon transform in studying wave dynamics. *Proceedings Coastal Dynamics* 2013.

Bell, P., 1999. Shallow water bathymetry derived from an analysis of X-band marine radar images of waves. *Coastal Engineering*, 37: 531-527.

Berni, C., Barthélemy, E. and Michallet, H., in press. Surf zone cross-shore boundary layer velocity asymmetry and skewness: an experimental study on a mobile bed. *Journal of Geophysical Research*.

De Bakker, A., Tissier, M., Marieu, V., Sénéchal, N., Ruju, A., Lara, J. and Ruessink, G., 2013. Infragravity-wave dissipation on a low-sloping beach. *Proceedings Coastal Dynamics* 2013.

De Bakker, A.T.M., Tissier, M.F.S. and Ruessink, B.G., sub judice. Shoreline dissipation of infragravity waves. *Continental Shelf Research.*

Elgar, S. and Guza, R.T., 1985. Observations of bispectra of shoaling surface gravity waves. *Journal of Fluid Mechanics*, 161: 425-448.

Guza, R.T. and Thornton, E.B., 1982. Swash oscillations on a natural beach. *Journal of Geophysical Research*, 87: 483-491.

Henderson, S.M., Guza, R.T., Elgar, S., Herbers, T.H.C. and Bowen, A.J., 2006. Nonlinear generation and loss of infragravity wave energy. *Journal of Geophysical Research*, 111, doi:10.1029/2006JC003539.

Herbers, T.H.C., Elgar, S. and Guza, R.T., 1994. Infragravity-frequency (0.005-0.05 Hz) motions on the shelf. Part I: Forced waves. *Journal of Physical Oceanography*, 24: 917-927.

Herbers, T.H.C., Elgar, S., Guza, R.T. and O'Reilly, W.C., 1995. Infragravity-frequency (0.005-0.05 Hz) motions on the shelf. Part II: Free waves. *Journal of Physical Oceanography*, 24: 917-927.

Herbers, T.H.C., Russnogle, N.R. and Elgar, S., 2000. Spectral energy balance of breaking waves within the surf zone. *Journal of Physical Oceanography*, 30: 2723-2737.

Lara, J.L., Ruju, A. and Losada, I.J., 2010. Reynolds averaged Navier-Stokes modelling of long waves induced by a transient wave group on a beach. *Proceedings of the Royal Society A*, doi:10.1098/rspa.2010.0331.

O'Donoghue, T. and Wright, S., 2004. Flow tunnel measurements of velocities and sand flux in oscillatory sheet flow for well-sorted and graded sands. *Coastal Engineering*, 51: 1163-1184.

Ribberink, J.S. and Al-Salem, A.A.,1994. Sediment transport in oscillatory boundary layers in cases of rippled beds and sheet flow. *Journal of Geophysical Research*, 99: 12707-12727.

Rocha, M., Silva, P.A., Michallet, H., Abreu, T. and Barthélemy, E., 2013. Nonlinearities of short and long waves across the shoaling, surf and swash zones: large-scale physical model results. *Proceedings Coastal Dynamics* 2013.

Ruessink, B.G., Kleinhans, M.G. and Van den Beukel, P.G.L., 1998. Observations of swash under highly dissipative conditions. *Journal of Geophysical Research*, 130: 3111-3118.

Ruessink, B.G., Michallet, H., Abreu, T., Sancho, F., Van der A, D.A., Van der Werf, J.J. and Silva, P.A., 2011. Observations of velocities, sand concentrations, and fluxes under velocity-asymmetric oscillatory flows. *Journal of Geophysical Research*, 116: doi:10.1029/2010JC006443.

Ruessink, B.G., Boers, M., Van Geer, P.F.C., De Bakker, A.T.M., Pieterse, A., Grasso, F. and De Winter, R.C., 2012. Towards a process-based model to predict dune erosion along the Dutch coast. *Netherlands Journal of Geosciences*, 91: 357-372.

Ruggiero, P., Holman, R.A. and Beach, R.A., 2004. Wave run-up on a high-energy dissipative beach. *Journal of Geophysical Research*, 109: doi.10.1029/2003JC002160.

Ruju, A., Lara, J.L., Michallet, H., Sénéchal, N. and Losada, I.J., 2013. Transient swash motions on a gently sloping beach. *Proceedings Coastal Dynamics* 2013.

Russell, P., 1993. Mechanisms for beach erosion during storms. *Continental Shelf Research*, 13: 1243-1265.

Sénéchal, N., Coco, G., Bryan, K.R. and Holman, R.A., 2011. Wave runup during extreme storm conditions. *Journal of Geophysical Research*, 116: doi:10.1029/2010JC006819.

Stockdon, H.F. and Holman, R.A., 2000. Estimation of wave phase speed and nearshore bathymetry from video imagery. *Journal of Geophysical Research*, 105: 22015-22033.

Thomson, J., Elgar, S., Raubenheimer, B., Herbers, T.H.C. and Guza, R.T., 2006. Tidal modulation of infragravity waves via nonlinear energy losses in the surfzone. *Geophysical Research Letters*, 33: doi:10.1029/2005GL025514.

Tissier, M., Bonneton, P., Almar, R., Castelle, B., Bonneton, N., and Nahon, A., 2011. Field measurements and non-linear prediction of wave celerity in the surf zone. *European Journal of Mechanics-B/Fluids*, 30: 635-641.

Tissier, M., Almar, R., Bonneton, P., Michallet, H., De Bakker, A. and Ruessink, G., 2013. Role of short and long-wave interaction on wave celerity in the surf zone of a low-sloping beach. *Proceedings Coastal Dynamics* 2013.

Van der A, D.A., O'Donoghue, T. and Ribberink, J.S., 2010. Measurements of sheet flow transport in acceleration-skewed oscillatory flow and comparison with practical formulations. *Coastal Engineering*, 57: 331-342.

Van der A, D.A., Mouazé, D., Vignal, L., Silva, P., Abreu, T., Barthélemy, E. and Michallet, H., 2013. Wave boundary layer dynamics on a low sloping laboratory beach. *Proceedings Coastal Dynamics* 2013.

Van Dongeren, A.R., Battjes, J., Janssen, T.T., Van Noorloos, J., Steenhauer, K., Steenbergen, G. and Reniers, A., 2007. Shoaling and shoreline dissipation of low-frequency waves. *Journal of Geophysical Research*, 112: doi:10.1029/2006JC003701.

Van Thiel de Vries, J.S.M., Van Gent, M.R.A., Walstra, D.J.R. and Reniers, A.J.H.M., 2008. Analysis of dune erosion processes in large-scale flume experiments. *Coastal Engineering*, 55: 1028-1040.

Yu. X., Hsu, T.J. and Hanes, D.M., 2010. Sediment transport under wave groups: relative importance between nonlinear wave shape and nonlinear boundary layer streaming. *Journal of Geophysical Research*, 115: doi:10.1029/2009JC005348.